Mechanical properties of unidirectional, porous polymer/ceramic composites for biomedical applications

Jordi Seuba[b], Eric Maire[b], Jérôme Adrien[b], Sylvain Meille[b], Sylvain Deville[a,*]

[a]*Université de Lyon, Université Claude Bernard Lyon 1, CNRS, Institut Lumière Matière, 69622 Villeurbanne, France*

[b]*Université de Lyon, INSA-Lyon, MATEIS CNRS UMR5510, Villeurbanne, France.*

Abstract

Ceramics are brittle, so imagine what porous ceramics are like. This weakness is often a major obstacle in many applications. The addition of a ductile phase such as a polymer to a porous ceramics can help overcome this intrinsic limitation. Yet, most studies so far have focused on the processing and characterization of dense composites, and to some extent to porous ceramic composites. Unidirectionality, with macropores arranged along a common direction, is another strategy to improve the strength of porous ceramics, while being beneficial for a wide range of other applications involved with mass, gas or species transport. Here we combine the two approaches and show a simple processing strategy to obtain highly porous, unidirectional ceramic/polymer composites. We infiltrated ice-templated porous zirconia scaffolds with a dilute solution of polymer (polycaprolactone or epoxy). After the evaporation of the solvent, porous ceramic composites with a porosity greater than 60% were obtained. We performed a complete mechanical characterization to assess the relative importance of the properties of the ceramic and polymer phases. Our results demonstrate that the addition of a ductile polymer (PCL) can increase both the strength and the tough-

---

*Corresponding author
Email address:* `sylvain.deville@univ-lyon1.fr` (Sylvain Deville)

ness of the composites while maintaining a high porosity. However, the addition of a brittle polymer (epoxy) has seemingly no impact on the fracture properties. This approach could provide porous materials that are easier to handle for biomedical applications.

---

1. Introduction

Highly porous ceramics are mostly used for their high permeability, low thermal conductivity, or open porosity which makes them useful in tissue engineering [1, 2], as catalyst supports [3], photocatalysis [4], oil/water separation [5], or in filtration applications [6]. However, their presence in technological fields where these functional properties have a crucial importance –energy harvesting, environment, or biomedicine– is still moderate. One of the main barriers to a wider application is the inherent brittleness of ceramic materials, resulting in brittle fracture at low load levels. Highly porous ceramics are often so weak that even their handling can be challenging.

The interplay between strength and toughness in ceramics make both properties mutually exclusive and has been a fruitful research area in the last decade. Extensive work has been done to improve the fracture toughness of ceramics with a moderate impact on strength. The explored strategies are as diverse as introducing residual compressive stresses [7], making stronger interfaces [8], introducing a polymeric [9] or metal phase [10], or mimicking the microstructure of natural composite materials [11, 12]. However, the majority of the research has been focused on dense ceramics and comparatively little has been done on their porous counterparts.

The most common approach to improve the mechanical properties of porous ceramics is the incorporation of a ductile organic phase [13], to partially or completely fill the porosity. It is nevertheless crucial to have a continuous ceramic scaffold first to provide strength and rigidity to the material. A coated ceramic scaffold is thus stronger and more rigid than a porous blend of materials where ceramic particles are distributed in the polymer phase. The ceramic scaffold provides high stiffness and stress resistance while the polymeric phase provides a higher flaw tolerance. One simple way to obtain such materials is to infiltrate a sintered or partially sintered ceramic with an organic phase. Because of their interest for biomedical applications, most studies have focused on biodegradable synthetic polymers as polycaprolactone (PCL) [14], polylactide-co- glycolide (PLGA) [15] or poly (D-L-lactic acid)(PDLLA) [16]. In all these studies, however, the initial porous structure was isotropic, with no preferential orientation of the macropores.

Ice-templating (or freeze-casting) is a processing technique for macroporous materials [17], investigated for its potential in applications as diverse as sensors [18], filtration [19], oil absorption [20], CO_2 capture and energy storage [21], microwave absorption [22], tissue engineering [23], oxygen transport membranes [24], sound adsorber [25], solid oxide fuel cells [26], or batteries [27]. The process consists in freezing particle suspensions, which induces a segregation of particles by the solidification front. After solidification, the frozen solvent is removed, leaving pores which morphologies are a replica of the sublimated crystals. Finally, the green body is sintered to consolidate the microstructure. A feature of this processing method that is both an advantage and a drawback is the mechanical anisotropy exhibited by the unidirectional macroporous structure, similar to honeycomb structures. Although this anisotropy offers a reinforcement in the direction parallel to the pores [28], the weaker resistance

in the perpendicular direction prevents their use in applications with a multiaxial stress field.

Several groups have infiltrated polymers into porous, ice-templated ceramic scaffolds, resulting in alumina/epoxy [29, 30], alumina/UDMA-TEGDMA [31], alumina/PMMA [32], or alumina/resin composites for dentistry applications [33]. These studies revealed the role of residual porosity–acting as defects and thus detrimental to the mechanical properties–as well as the role of the mechanical properties of the polymer phase and its adhesion to the ceramic surface. Without a good adhesion (e.g., with epoxy), delamination occurs easily at the polymer/ceramic interface [29, 30]. A better control of the adhesion can be achieved with PMMA [32]. However, in all these studies, the final composites are nearly dense, with a residual porosity of only a few percents.

Comparatively, relatively little studies can be found on the processing and mechanical properties of anisotropic, highly porous ceramic/polymer composites. The only study addressing the processing and characterization of highly porous ice-templated porous composites is the work of Flauder *et al.* [34]. Ice-templated calcium phosphates (TCP) scaffolds were infiltrated with a low amount (1–5%) of polycaprolactone (PCL), to obtain materials for bone replacement applications. The objective was thus to improve the mechanical properties (strength, toughness) of the material while preserving the open and directional macroporosity for cells penetration. Several infiltration cycles were performed to fill the micropores within the ceramic walls and ultimately create a thin polymer coating at the surface of the ceramic walls. A noticeable improvement of strength and damage tolerance was observed, due to the elastic and plastic deformation of the polymer, as expected, but also formation of polymer fibrils creating local bridges in the structure. The surprising increase in strength was possibly explained by the cold drawing and hardening of PCL fibers during failure. PCL fibers pro-

vide load transfer capacities to the structure, across the crack flanks, decreasing stress level at the crack tip. Both the compressive and flexural strength values were reported.

Here, we followed a similar approach with a stronger ceramic (yttria-stabilized zirconia) and investigated the mechanical properties of highly porous ceramic-polymer composites with unidirectional porosity. We developed a route to process such composites by partially infiltrating ice-templated scaffolds with a dilute polymer solution. We characterized the impact of polymer infiltration on microstructure and mechanical properties (flexural strength, work of fracture, toughness), and assessed the effect of two polymers with different mechanical behaviors: brittle (Epoxy) or ductile (PCL). We characterized the damage mechanisms by bending some of our notched samples in situ in a laboratory tomograph.

2. Materials and Methods

2.1. Processing the composite

Ceramic scaffolds with unidirectional porosity were produced by ice-templating as described in previous work [28]. First, water-based solutions were prepared by mixing 3 mol.% yttria-stabilized zirconia (TZ-3YS, Tosoh, Tokyo, Japan) at 50 wt.% solid loading, 0.75 wt.% of dispersant (Prox B03, Synthron, Levallois-Paris, France), and 3 wt.% of organic binder PVA (PVA2810, Wacker, Burghausen, Germany). All the percentages are referred to the total solid content of the dispersion. Afterwards, the slurry was ball milled (24 hrs), magnetically stirred, and deaired (15 min).

Ice-templating was performed by pouring 10 ml of slurry into a PTFE mold (20 mm diameter and 25 mm height) placed on top of a copper plate and freezing from the bottom to the top. The temperature was controlled by circulating

silicone oil regulated by a cryothermostat (Model CC 905, Hubert, Offenburg, Germany) through the copper plate. The cooling rate was set at 2°C/min. After complete solidification, samples were demolded and freeze-dried for at least 48 hrs in a commercial freeze-dryer (Free Zone 2.5 Plus, Labconco, Kansas City, Missouri, USA).

The subsequent sintering cycle involved first removal of organic components, which was achieved by heating the samples from room temperature to 500°C at a rate of 3°C/min and holding them at this temperature for 5 hrs. Then, samples were sintered at 1400°C (heating rate of 5°C/min) for 3 hrs. 2 mm of the bottom of each sample were cut off to remove the portion of the samples with an initial porosity gradient [35]. Finally, between 5 to 8 bars were cut from each ice-templated monolith with dimensions of $14 \times 3 \times 3$ mm^3 and a longitudinally oriented porosity.

Sintered ice-templated bars were infiltrated with two different polymers, polycaprolactone (Polycaprolactone Aldrich 440744-500G, M$_n$ = 80,000 g/mol, Sigma-Aldrich) or epoxy (Epotek 301, Billerica, Massachussetts, USA). The PCL infiltration process consisted in the preparation of PCL solutions with different concentration (4 and 8 wt.%) in ethyl acetate (anhydrous, 99.8%, Sigma-Aldrich) at 80°C. Afterwards, the specimens were placed in a PTFE mold and the PCL solution poured on it. The process was performed under vacuum to facilitate the infiltration and removal of the residual air entrapped in the samples. After 20 min of vacuum infiltration the samples were placed on an absorbent paper for 24 hrs to ensure the entire evaporation of the solvent. Infiltration with epoxy was performed following a similar procedure: a mix of resin and hardener (80–20 wt.% respectively) was poured under vacuum in a PTFE mold with the ice-templated bars on it. Afterwards, the excess of epoxy was removed from the samples using a tabletop centrifuge at different centrifugal speeds (2500, 5000, 7500, and

10000 rpm).

2.2. Characterization

The apparent density of ice-templated bars (ρ) was measured as total weight divided by external volume (V). The porosity (P) was determined from these measurements by considering 6.05 g/cm^3 as theoretical density (ρ_0) for YSZ. The porosity was determined from the apparent density as:

$$P(\%) = 1 - \frac{\rho}{\rho_0} \tag{1}$$

The volume (OC) of the scaffold occupied by the organic after infiltration was determined by:

$$OC(\%) = \frac{m_1 - m_0}{\rho_{organic} \cdot V} \tag{2}$$

where m_1 is the mass of the infiltrated sample after solvent evaporation and $\rho_{organic}$ is the theoretical density of the infiltrated organic (ρ_{PCL} = 1.145 g/cm^3 and ρ_{Epoxy} = 1.25 g/cm^3). Microstructural characterization was investigated on fracture surfaces by scanning electron microscopy (FEI XL30 ESEM FEG).

Flexural strength (Eq. 3) of infiltrated and non-infiltrated bars was evaluated in a 4-points bending test using a hydraulic universal testing machine (Instron 8502) equipped with a 10 kN cell load at a constant cross-head speed of 0.2 mm/min. The sample deflection was measured by a linear variable differential transformer (LVDT) with micrometer accuracy. The flexural strength σ_f is given by:

$$\sigma_f = \frac{3F(L - L')}{4bh^2} \tag{3}$$

where F is the applied load, b and h the width and height of the sample, L and L'

7

the respective lower an upper span. The fracture toughness (K_{Ic}) was calculated by Eq. 4, from tests on notched samples:

$$K_{Ic} = Y\sigma_f\sqrt{\pi a} \tag{4}$$

where σ_f is the flexural stress, $Y = 1.64$ a geometrical factor, and a is the notch length. Work of fracture G values were obtained from the curves obtained during the 4-points bending test measuring the area below the force-displacement curve up to the maximum stress (G_{max}) or to a given value of strain ($G_{7\%}$ on typically $18 \times 3 \times 4 mm^3$ samples) divided by the remaining sample section in notched samples.

2.3. X-Ray Tomography

X-ray tomography was used to image the crack path *in situ* and better understand the role of the microstructural features on the crack propagation. Of particular interest was the role of the orientation domains of the lamellar structure of ice-templated samples [36, 37]. Because of the high absorption of X-rays by zirconia, we could not image cracks in zirconia composites. We choose instead to prepare similar composites from ice-templated alumina, the later having a much lower absorption coefficient. Ice-templated alumina samples were prepared with the exact same conditions than these previously described in YSZ, yielding similar microstructure. We developed a simple setup for the tomograph to initiate and propagate a crack *in situ* in a bent, notched sample (see the radiograph shown in Fig. 1). The notched sample is placed between two fixtures, inside a custom compression testing device, described in [38]. The sample is clamped in the fixed lower fixture, while its upper part is in contact with the inclined surface of the upper fixture. A vertical displacement of this inclined surface induces a bending stress on the sample, and thus initiates the propagation of the crack. The crack

in the notch area remains at an almost constant position, which facilitates the imaging. Although we cannot precisely estimate the stress level on the sample, this approach let us identify the role of the orientation domains on the crack propagation, for which the exact stress level is not needed.

The imaging was performed on a Vtomex tomograph (GE Phoenix X-ray Gmbh) operated at 90 keV, 240 μA intensity. For these measurements, 1000 radiographs were recorded during the 360 degrees rotation with an exposure time of 333 ms each, resulting in an acquisition time of roughly 20 min. The obtained voxel size was 3 μm.
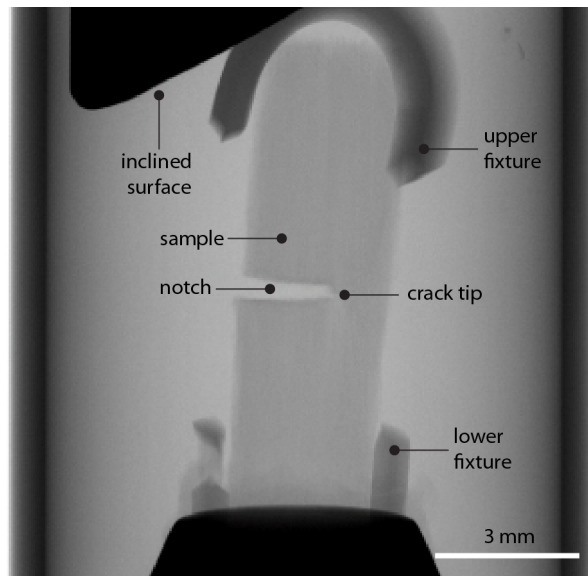

Figure 1: Detail of the sample and set-up used for the in-situ bending test in the X-ray tomograph. The notched sample is placed vertically between two fixtures. Because of the inclined surface, the displacement of the upper fixture bends the sample, which eventually initiates a crack.

3. Results and discussion

3.1. YSZ/PCL composites

Ice-templating allows the processing of YSZ samples with reproducible microstructure and porosity. The sintered ceramic monoliths fabricated in this study have a total porosity of 77.1 $\pm$ 1.5 % and the scaffolds that were cut off from these same

monoliths exhibit a comparable total porosity of 78.2 ± 0.7 %. This slight decrease of porosity when removing the lower part of the sample can be explained by the higher density of this initial region. The velocity of the ice front in the transient regime is high, which results in the engulfment of a larger fraction of particles–and thus a lower porosity in the final material [35]. Sedimentation may also explain this slight decrease of porosity in this region.

Fig. 2-A shows a close-up view, as observed on SEM micrographs, of the unidirectional porosity created by the ice-templating process with rough walls that replicates the dendritic morphology of the ice crystals. After infiltration by a 4 wt.% PCL solution (1 cycle), a thin polymer layer is homogeneously deposited on the ceramic walls without filling the porosity (Fig. 2-B).
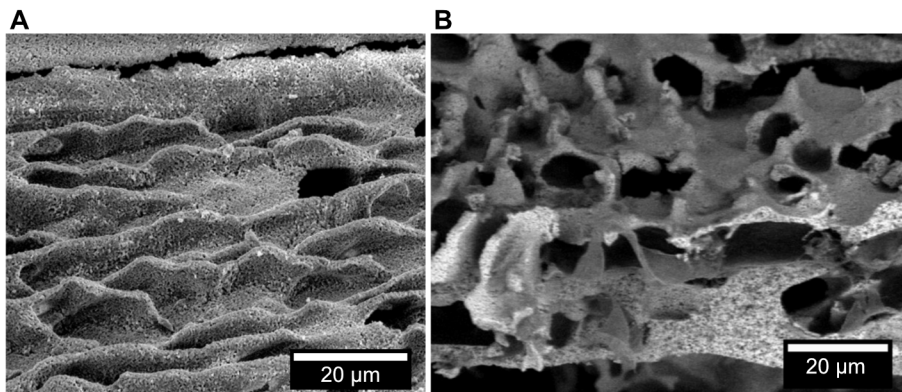

Figure 2: SEM micrographs of ice-templated YSZ before (A) and after (B) infiltration by a 4wt.% PCL solution. Only a thin polymer layer is deposited at the surface, the directional macropores are still open. © (2020) J. Seuba *et al.* (10.6084/m9.figshare.15022263) CC BY 4.0 license https://creativecommons.org/licenses/by/4.0/.

We investigated the effect of PCL infiltration on porosity (Table 1). As expected, the measured organic content increased with the number of infiltration cycles. In samples infiltrated with a 4wt.% PCL solution, the organic content increases from 4.0% to 10.1% when the number of cycles increases from 1 to 4. Conversely, the porosity decreases linearly with the number of infiltration cycles, as shown in Fig. 3.

Specimens where the amount of PCL initially infiltrated in the specimens is the

same (4×4wt.% PCL vs 2×8wt.% PCL and 2×4wt.% PCL vs 1×8wt.% PCL) exhibited a comparable measured organic content and porosity. We did not investigate infitrations with more concentrated polymer solutions, as the increase of the viscosity with the PCL concentration became problematic. A more viscous solution is more difficult to deposit homogeneously and thus creates clogged pores, as reported by Peroglio et al. [39] in porous biphasic calcium phosphates processed by organic burn-out and similar PCL infiltration conditions. Our results are also in agreement with the optimal conditions determined by Flauder *et al.* [34], who selected 4wt.% as the optimal PCL concentration in acetone for infiltration. Although this choice was not justified by the authors, it is likely related to the same infiltration constraints. Despite the solvent in both studies being different, a too high polymer concentration is deleterious for this infiltration approach.

We can also note, from the porosity values reported in table 1, that the standard deviation values of the porosity are small (less than 1%). Porosity differences between similar samples have two possible origins: differences in the amount of porosity in the ice-templated ceramic scaffolds, and different outcomes of the polymer infiltration procedure (repeated in some cases up to 8 times). Ice-templating is a robust approach: when the same suspension is frozen under the same conditions to prepare several samples, the final porosity range (after drying and sintering) is narrow, typically within 1% [28]. This value is similar to the values measured in the final composites, which therefore indicate that the polymer infiltration procedure is quite robust too, and produce consistent results between samples infiltrated in similar conditions.

PCL concentration (wt.%)	Cycles	Total porosity (%)	Ceramic content (%)	Organic content (%)
0	0	78.4 ± 2.9	21.6 ±0.9	0
4	1	75.8 ± 1.0	20.2 ±0.8	4.0 ±0.06
4	2	73.5 ± 0.4	19.9 ±0.3	6.6 ±0.3
4	3	70.7 ± 0.1	19.2 ±0.7	10.1 ±0.7
4	4	66.5 ± 2.6	20.6 ±0.7	12.9 ±2.3
8	1	73.3 ± 0.8	21.6 ±0.7	6.0 ±0.4
8	2	67.0 ± 1.8	20.5 ±0.6	12.5 ±1.2

Table 1: Open and close porosity of PCL/YSZ composites for different number of infiltration cycles and different PCL concentration of the infiltration solution.
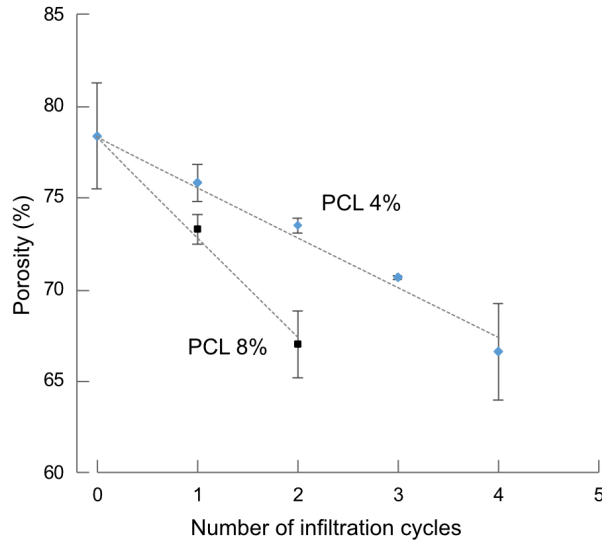

Figure 3: Porosity content vs. number of infiltration cycles, for PCL solutions with different PCL concentrations. Dashed lines are a guide for the eyes. © (2020) J. Seuba *et al.* (10.6084/m9.figshare.15022263) CC BY 4.0 license https://creativecommons.org/licenses/by/4.0/.

Fig. 4 shows representative stress-strain curves for ice-templated bars with no infiltration, 1 infiltration cycle, and 4 infiltration cycles (4% PCL solution) in a 4-points bending test. The non-infiltrated specimens show the typical response of a porous ceramic material, with an elastic behavior until catastrophic failure. Some fracture events may occur before the maximum stress is reached, leading to the stochastic shape of the compression curve. These events are most likely caused by the fracture of the internal struts in the porous structure.
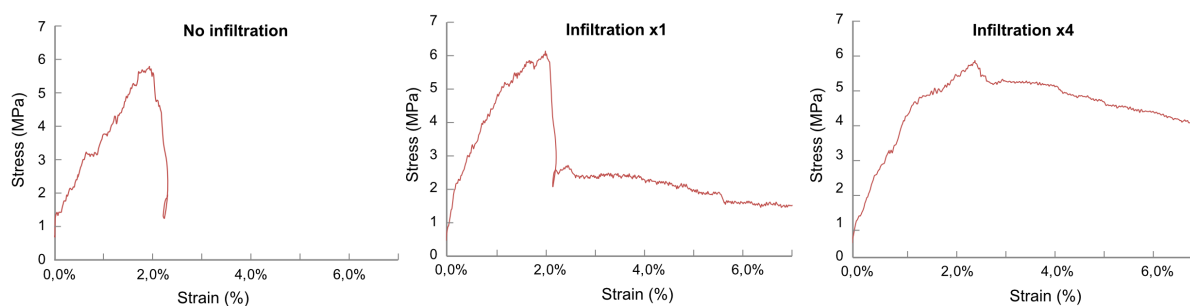
Figure 4: Stress-strain curves during mechanical testing (bending) of un-notched bars for the porous ceramic (left), and for the PCL/ceramic composites after 1 infiltration (middle) and 4 infiltration cycles (right). Infiltration with a 4% PCL solution. Note the displacement is measured by an LVDT sensor and not by the displacement of the fixture, explaining thus why the strain value may go backwards (center plot, around 2%). © (2020) J. Seuba *et al.* (10.6084/m9.figshare.15022263) CC BY 4.0 license https://creativecommons.org/licenses/by/4.0/.

Both PCL-infiltrated scaffolds (1 and 4 infiltration cycles) show a linear elastic behavior in the first stage, similar to non-infiltrated samples. However, once the ceramic is broken (at the end of the linear elastic region), polymer-infiltrated scaffolds exhibited a plastic stage (plateau) at a load level which depends on the amount of polymer in the porous composite. This effect is also quantified by the work of fracture differences obtained in each infiltration condition at a similar strain value of 7% (as calculated using the linear elastic assumption) (Tab. 2). For instance, samples infiltrated 4 times exhibited a $G_{7\%}$ significantly higher than the samples infiltrated only once (203 $J \cdot m^{-2}$ vs. 97 $J \cdot m^{-2}$).

The impact of the amount of polymer on fracture toughness (K_{Ic}), and work of fracture at maximum stress (G_{max}) is noticeable (Tab. 2). The toughness K_{Ic}, for example, is twice greater after 4 infiltration cycles ($0.40 MPa \cdot m^{1/2}$ after infiltration vs. $0.23 MPa \cdot m^{1/2}$ before), despite a low amount of polymer introduced in the structure. This implies that the initiation of the fracture is not determined by just the amount of ceramic in the scaffold, since this amount is the same for the three conditions (0, 1 and 4 infiltration cycles). The addition of a polymer improved all the mechanical properties reported here. Once the fracture is initiated, the amount of organic phase also controls the resistance to crack

propagation, as evidenced by the increase of $G_{7\%}$ values with infiltration cycles.

This improvement of properties has several possible origins, the most likely one being the redistribution of stress in the solid phase as well as a strengthening of the walls, as reported previously [34]. This behaviour is not observed in dense ceramic/polymer composites [40], where the presence of a soft polymer has no positive effect on the initiation of fracture.

Infiltration cycles	σ_f (MPa)	Strain at failure (%)	$K_{Ic}(MPa \cdot m^{1/2})$	$G_{max}(J \cdot m^{-2})$	$G_{7\%}(J \cdot m^{-2})$
0	4.71 ± 0.78	2.11 ± 0.41	0.23 ± 0.04	35 ± 7	-
1	5.79 ± 0.40	2.39 ± 0.39	0.26 ± 0.03	41 ± 12	97 ± 18
4	6.54 ± 1.13	2.65 ± 0.42	0.40 ± 0.03	66 ± 13	203 ± 33

Table 2: Mechanical properties of the porous ceramic and PCL-infiltrated composites (1 and 4 infiltration cycles with a 4wt.% PCL solution). 5 samples were tested for each condition. σ_f and strain at failure: Un-notched samples. K_{Ic}, G_{max} and $G_{7\%}$: notched samples.

Besides the effects on the mechanical properties (crack propagation), polymer infiltration also affects the handling and integrity of the specimens. While non-infiltrated samples formed a lot of debris and collapse in multiple parts during mechanical testing, the PCL-infiltrated ones retained good integrity even when damaged (Fig. 5). Unfortunately, it was not possible to evaluate the maximum deformation before final fracture because the samples came into contact with the sample holder. Peroglio et al. [14] reported residual deflection higher than 1 mm (for a sample size of $6 \times 10 \times 60 \ mm^3$) before total fracture in samples with comparable microstructures.

Figure 5: Samples after mechanical testing. Porous ceramic (left) and composite after 1 (middle) and 4 (right) infiltration cycles. The porous composites are still holding as one piece after testing. The samples are from the tests reported in Fig. 4. © (2020) J. Seuba *et al.* (10.6084/m9.figshare.15022263) CC BY 4.0 license https://creativecommons.org/licenses/by/4.0/.

The toughening effect obtained is intrinsic to the introduction of a highly deformable polymeric phase, which holds the structure together even when the ceramic structure collapses [41]. This mechanism is analogous to the extensively reported crack bridging effect observed in cancellous bone [42, 43]. In the first stage, the ceramic scaffold withstands the stresses until its failure at a limited strain. Afterwards, in the plastic stage, the polymer phase controls the crack propagation until the polymer reaches its characteristic elongation to fracture producing a crack bridging effect. In our samples, PCL fibrils act in ice-templated scaffolds (see Fig. 6 for a SEM micrograph of these fibrils in our material after fracture) like collagen fibrils in human bone. A similar effect has been shown by Currey et al. [44], who observed that the post-yield strain of bone is highly dependent on collagen content. The key mechanism responsible for the improvement of the mechanical properties in these highly porous materials is therefore the load redistribution enabled by the continuous polymer phase.
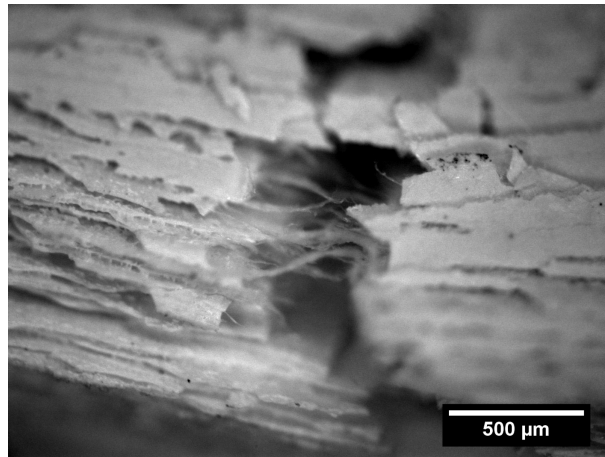

Figure 6: Close-up view of crack bridging by PCL fibrils after crack propagation in a PCL/YSZ composite. © (2020) J. Seuba *et al.* (10.6084/m9.figshare.15022263) CC BY 4.0 license https://creativecommons.org/licenses/by/4.0/.

3.2. YSZ/Epoxy composites

Fig. 7 shows micrographs of YSZ ice-templated scaffolds after the epoxy impregnation and centrifugation. Similarly to the PCL infiltrated samples, the epoxy is deposited onto the rough ceramic walls without filling the microporosity. How-

ever, the epoxy is too viscous to be removed from the samples, which generates a clogged porosity in some parts of the sample.
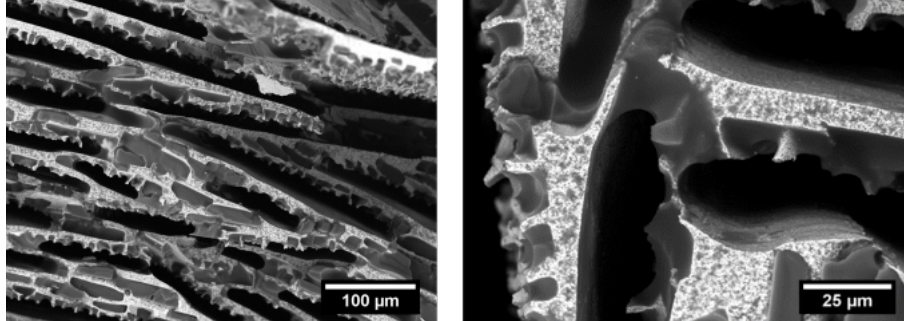

Figure 7: SEM micrographs of epoxy/YSZ composites. Because of its higher viscosity, the epoxy is not deposited homogeneously through the sample. Small macropores are filled with epoxy. © (2020) J. Seuba *et al.* (10.6084/m9.figshare.15022263) CC BY 4.0 license https://creativecommons.org/licenses/by/4.0/.

We investigated the effect of centrifugal speed on porosity (Table 3). The porosity increases with the centrifugal speed (Fig. 8). The infiltrated polymer is more easily removed from the sample as the centrifugal speed increases. It is thus a simple way to control the amount of polymer deposited into the porous ceramic scaffold.

Centrifugal speed	Ceramic content (%)	Polymer content (%)	Porosity (%)	σ_f (MPa)
2500	20.7 ± 1.0	34.5 ± 5.2	44.8 ± 5.1	26.1 ± 4.0
5000	20.0 ± 0.8	27.2 ± 0.3	52.9 ± 0.3	15.0 ± 5.8
7500	20.0 ± 0.8	22.1 ± 1.0	58.0 ± 1.0	12.1 ± 4.1
10000	22.2 ± 0.9	15.2 ± 1.4	62.5 ± 1.5	8.8 ± 2.0

Table 3: Variation of porosity with centrifugal speed after infiltration of the epoxy into the YSZ samples. YSZ/epoxy composites
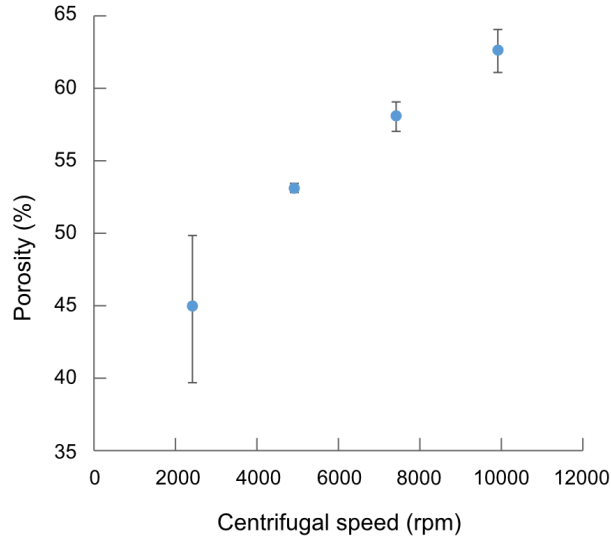
.

Figure 8: Porosity content (%) vs. centrifugal speed (rpm) after infiltration of the epoxy into the YSZ samples. © (2020) J. Seuba *et al.* (10.6084/m9.figshare.15022263) CC BY 4.0 license https://creativecommons.org/licenses/by/4.0/.

During the 4-points bending tests, epoxy-YSZ composites exhibited a typical brittle linear elastic behavior similar to non-infiltrated samples. The flexural strength of the specimens centrifuged between 2500 rpm and 10000 rpm ranges from 26.0 MPa to 8.8 MPa, for samples with porosities varying from 44.8% and 62.5% (Tab. 3). The porosity in turn controls the strength of the epoxy-based composites. At low centrifugation speed, the centrifugal forces are not enough to spread and remove the epoxy from the sample. The epoxy therefore completely fills parts of the pores. This type of defect affects the microstructural homogeneity of the sample and increases the effective area that withstands the load.

Sample	Ceramic content (%)	Polymer content (%)	Porosity (%)	σ_f (Mpa)	Note
YSZ	21.6 ± 0.9	-	78.4 ± 2.9	3.0 ± 1.8	
YSZ/PCL	20.6 ± 0.7	12.9 ± 2.3	66.5 ± 2.6	6.5 ± 1.1	4 infiltrations
YSZ/epoxy	22.2 ± 0.9	15.2 ± 1.4	62.5 ± 1.5	8.8 ± 2.0	1000rpm
YSZ/epoxy/PCL	21.9 ± 0.6	15.6 ± 1.2	62.5 ± 1.4	11.3 ± 3.2	10000 rpm + 1 infiltration 4%

Table 4: Variation of porosity and flexural strength of the various composites (YSZ/PCL, YSZ/epoxy, and YSZ/PCL/epoxy).

.

We further explored the possibility to modify simultaneously crack initiation and propagation by infiltrating both polymers in two steps. First, the ceramic samples were infiltrated with epoxy with the procedure previously described. Second, the epoxy-YSZ porous composite was vacuum-infiltrated with a PCL solution. As we expected, the resultant microstructure exhibited an epoxy layer which does not bond with the ceramic scaffold, and a PCL coating on top of that (Fig. 9). The mechanical properties are only marginally improved by the dual infiltration (Tab 4). The YSZ/epoxy composites, however, show a brittle behavior while the dual infiltrated samples are more ductile.
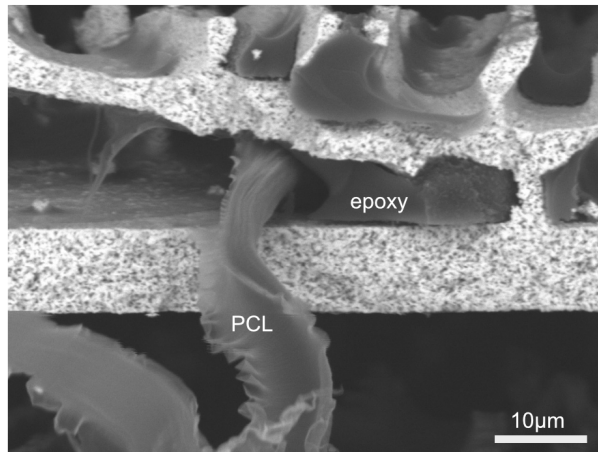

Figure 9: Close-up view of the fracture surface of a PCL/epoxy/YSZ porous composite. The different fracture behavior of the two polymers can clearly be observed: the epoxy fails in a brittle manner, while the PCL creates elongated fibrils upon failure. © (2020) J. Seuba *et al.* (10.6084/m9.figshare.15022263) CC BY 4.0 license https://creativecommons.org/licenses/by/4.0/.

3.3. In situ X-ray computed tomography of bending test

Little is known about the fracture behavior of such porous, anisotropic composites in bending. We previously investigated the role of the polymer phase. In order to better understand the mechanical response of PCL-ceramic composites, we performed a bending test *in situ* in a X-Ray tomograph. The polymer phase is too light (not enough absorption) to appear on the X-ray images, but the goal here is to understand the role of the ceramic microstructural feature. Fig. 10 shows a 3D reconstruction of the sample, where the notch and the crack and its

path can clearly be identified.

The structure of ice-templated materials is typically defined by two features. At a small scale, a lamellar microstructure, replicating the morphology of the ice crystals, is observed. On a short-range, adjacent lamellaes are parallel to each other. On a longer range, the lamellaes are organized in so-called orientation domains, where all the lamellaes are parallel to each other within a domain. Unless specific processing tricks are used (freezing under flow [11], applying magnetic fields during freezing [45], etc.), orientation domains have been observed to be randomly oriented, because of the random selection of the ice crystals in the first instants of freezing. The characteristics of the orientation domains directly impact the mechanical response of the ice-templated materials [36].

The lamellar orientation domains were color-coded based on their orientation (using the *Directionality* plugin of Fiji [46]) to facilitate the identification of their boundaries. Once the crack is initiated at the tip of the notch, it propagates in different directions depending on the orientation of the domains it encounters, along the boundaries of the orientation domain. This propagation path is intra-domain when the pores in the domain are favorably oriented. A strong change in crack direction is observed at the domain boundary (A marks in Fig. 10). Because of the presence of orientation domains, there is not a single weak direction in the material. This behavior increases the crack tortuosity. These results are in good agreement with the role of orientation domains identified by Lichtner *et al.* [36] in 1D compression tests. This extrinsic mechanism, coupled with the crack bridging provided by the PCL, adds an additional toughening mechanism to the material.

The results that we present in this section are preliminary, and we have to further explore this mechanisms and investigate the particular role of other microstructural features such as the pore/wall ratio, the pore directionality, or the size of

the orientation domains. These results nevertheless show that the orientation domains play a role on crack propagation and that the current approach can be used to better understand these mechanisms.
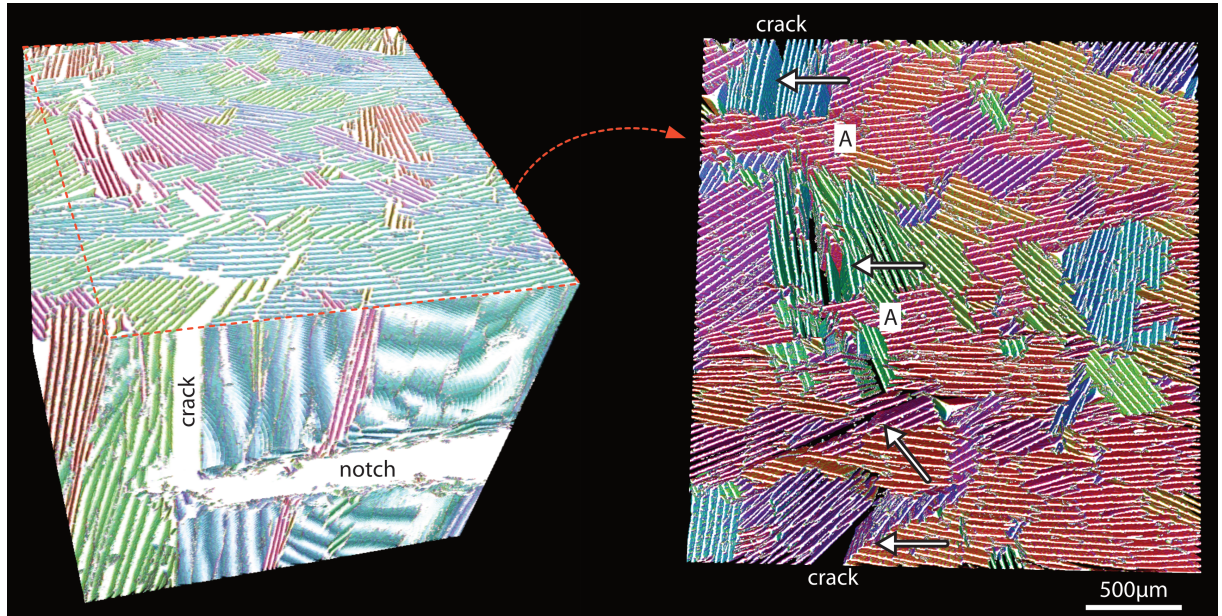

Figure 10: X-Ray 3D reconstruction of a PCL-alumina composite during the in situ bending test. The color code indicates the local orientation of the domain, which helps delineate the boundaries of the domains. The notch can be seen on the left image. The crack (arrows) can be seen on the images. The crack followed the weakest direction, along the lamellar walls. The existence of domains with different orientations favours the crack deflection. Crack bridging by orientation domains (A), oriented perpendicular to the crack, can be observed. © (2020) J. Seuba *et al.* (10.6084/m9.figshare.15022263) CC BY 4.0 license https://creativecommons.org/licenses/by/4.0/.

4. Conclusions

Here we prepared and characterized porous ceramic/polymer composites with high open porosity contents (>70%). We characterized the effect of different experimental conditions (infiltration cycles, polymer concentration, centrifugal speed) on the mechanical response. We showed that the nature of the polymer (brittle or ductile) may change the fracture behavior of ice-templated porous composites. PCL has a moderate impact only on properties linked to crack initiation (flexural strength, fracture toughness, strain), as already shown for dense ceramic/organic composites by Niebel *et al.* [47], but a strong impact on the crack propagation (strain energy release and strain to failure). In contrast, epoxy

infiltration does not change the fracture behavior (brittle fracture) of porous composites although the flexural strength is slightly improved. No adhesion was found between the polymer and its ceramic substrate. Improving the adhesion by a chemical bounding (grafting) could certainly further improve the mechanical properties. These results are encouraging since the approach is applicable to other systems such as hydroxyapatite/PCL that could be used for synthetic bone substitutes. An increase of the energy stored for the material before total failure could increase the mechanical stability and facilitate their handling and transport, while maintaining an open porosity.

Acknowledgements

References

[1] T. Ohji, M. Fukushima, Macro-porous ceramics: processing and properties, Int. Mater. Rev. 57 (2012) 115–131.

[2] K. Okada, T. Isobe, K.-i. Katsumata, Y. Kameshima, A. Nakajima, K. J. D. MacKenzie, Porous ceramics mimicking nature-preparation and properties of microstructures with unidirectionally oriented pores, Sci. Technol. Adv. Mater. 12 (2011) 064701.

[3] A. Julbe, D. Farrusseng, C. Guizard, Porous ceramic membranes for catalytic reactors-overview and new ideas, Journal of Membrane Science 181 (2001) 3–20.

[4] Z. Xing, W. Zhou, F. Du, L. Zhang, Z. Li, H. Zhang, W. Li, Facile synthesis of hierarchical porous tio2 ceramics with enhanced photocatalytic performance for micropolluted pesticide degradation, ACS applied materials & interfaces 6 (2014) 16653–16660.

[5] Y. Bi, L. Han, Y. Zheng, Y. Guan, H. Zhang, S. Ge, H. Wang, Q. Jia, Y. Zhang, S. Zhang, Lotus-seedpod-bioinspired 3d superhydrophobic diatomite porous ceramics comodified by graphene and carbon nanobelts, ACS applied materials & interfaces 10 (2018) 27416–27423.

[6] E. C. Hammel, O.-R. Ighodaro, O. I. Okoli, Processing and properties of advanced porous ceramics: An application based review, Ceramics International 40 (2014) 15351–15370.

[7] R. Bermejo, C. Baudin, R. Moreno, L. Llanes, A. Sanchez-Herencia, Processing optimisation and fracture behaviour of layered ceramic composites with highly compressive layers, Compos. Sci. Technol. 67 (2006) 1930–1938.

[8] S. Bueno, C. Baudín, Composites : Part A Design and processing of a ceramic laminate with high toughness and strong interfaces, Composites Part A 40 (2009) 137–143.

[9] F. J. Martinez-Vazquez, A. Pajares, F. Guiberteau, P. Miranda, Effect of polymer infiltration on the flexural behavior of β-tricalcium phosphate robocast scaffolds, Materials 7 (2014) 4001–4018.

[10] C. Ferraro, S. Meille, J. Réthoré, N. Ni, J. Chevalier, E. Saiz, Strong and tough metal/ceramic micro-laminates, Acta Mater. 144 (2018) 202–215.

[11] F. Bouville, E. Maire, S. Meille, B. Van de Moortèle, A. J. Stevenson, S. Deville, Strong, tough and stiff bioinspired ceramics from brittle constituents., Nat. Mater. 13 (2014) 508–14.

[12] M. E. Launey, E. Munch, D. H. Alsem, H. B. Barth, E. Saiz, A. P. Tomsia, R. O. Ritchie, Designing highly toughened hybrid composites through nature-inspired hierarchical complexity, Acta Materialia 57 (2009) 2919–2932.

[13] D. Mohamad Yunos, O. Bretcanu, A. R. Boccaccini, Polymer-bioceramic composites for tissue engineering scaffolds, Journal of Materials Science 43 (2008) 4433–4442.

[14] M. Peroglio, L. Gremillard, J. Chevalier, L. Chazeau, C. Gauthier, T. Hamaide, Toughening of bio-ceramics scaffolds by polymer coating, Journal of the European Ceramic Society 27 (2007) 2679–2685.

[15] X. Miao, D. M. Tan, J. Li, Y. Xiao, R. Crawford, Mechanical and biological properties of hydroxyapatite/tricalcium phosphate scaffolds coated with poly(lactic-co-glycolic acid), Acta Biomaterialia 4 (2008) 638–645.

[16] S. Novak, J. Druce, Q. Z. Chen, A. R. Boccaccini, TiO2 foams with poly-(d,l-lactic acid) (PDLLA) and PDLLA/Bioglass® coatings for bone tissue engineering scaffolds, Journal of Materials Science 44 (2009) 1442–1448.

[17] S. Deville, Ice-Templating: Processing Routes, Architectures, and Microstructures, in: Freez. Colloids Obs. Princ. Control. Use, Springer International Publishing, 2017, pp. 171–252.

[18] J. Huang, J. Zeng, B. Liang, J. Wu, T. Li, Q. Li, F. Feng, Q. Feng, M. J. Rood, Z. Yan, Multi-Arch-Structured All-Carbon Aerogels with Superelasticity and High Fatigue Resistance as Wearable Sensors, ACS Appl. Mater. Interfaces 12 (2020) 16822–16830.

[19] J. Seuba, S. Deville, C. Guizard, A. J. Stevenson, Gas permeability of ice-templated, unidirectional porous ceramics, Sci. Tech. Adv. Mater. 17 (2016) 313–323.

[20] chenyang Cai, Z. Wei, Y. Huang, C. Ding, P. Wang, J. Song, L. Deng, Y. Fu, W.-H. Zhong, Ultralight Programmable Bioinspired Aerogels with Integrated Multi-functional Surface for Self-cleaning, Oil Absorption, and Thermal Insulation via Co-assembly, ACS Appl. Mater. Interfaces (2020) acsami.0c00308.

[21] S. Geng, J. Wei, S. Jonasson, J. Hedlund, K. Oksman, Multifunctional Carbon Aerogels with Hierarchical Anisotropic Structure Derived from Lignin and Cellulose Nanofibers for CO2 Capture and Energy Storage, ACS Appl. Mater. Interfaces (2020) acsami.9b19955.

[22] J.-b. Cheng, H.-b. Zhao, M. Cao, M.-E. Li, A.-n. Zhang, S.-l. Li, Y.-z. Wang, Banana Leaf-Like C-doped MoS2 Aerogels Towards Excellent Mi-

crowave Absorption Performance, ACS Appl. Mater. Interfaces (2020) ac-sami.0c01841.

[23] S. Deville, E. Saiz, A. P. Tomsia, Freeze casting of hydroxyapatite scaffolds for bone tissue engineering., Biomaterials 27 (2006) 5480–9.

[24] C. Gaudillere, J. Garcia-Fayos, M. Balaguer, J. M. Serra, Enhanced Oxygen Separation through Robust Freeze-Cast Bilayered Dual-Phase Membranes., Chem. Sus Chem. 7 (2014) 2554–61.

[25] J.-H. Oh, J. Kim, H. Lee, Y. Kang, I.-K. Oh, Directionally Antagonistic Graphene Oxide-Polyurethane Hybrid Aerogel as a Sound Absorber, ACS Appl. Mater. Interfaces 10 (2018) 22650–22660.

[26] A. Lichtner, D. Jauffrès, C. L. Martin, R. K. Bordia, Processing of Hierarchical and Anisotropic Porosity LSM-YSZ Composites, J. Am. Ceram. Soc. 96 (2013) 2745–2753.

[27] H. Zhai, P. Xu, M. Ning, Q. Cheng, J. Mandal, Y. Yang, A Flexible Solid Composite Electrolyte with Vertically Aligned and Connected Ion-Conducting Nanoparticles for Lithium Batteries, Nano Lett. 17 (2017) 3182–3187.

[28] J. Seuba, S. Deville, C. Guizard, A. J. Stevenson, Mechanical properties and failure behavior of unidirectional porous ceramics, Scientific Reports 6 (2016) 1–11.

[29] S. Deville, E. Saiz, R. K. Nalla, A. P. Tomsia, Freezing as a Path to Build Complex Composites, Science 311 (2006) 515 –518.

[30] J. Roleček, D. Salamon, Z. Chlup, Mechanical properties of hybrid composites prepared by ice-templating of alumina, J. Eur. Ceram. Soc. 37 (2017) 4279–4286.

[31] S. Al-Jawoosh, A. Ireland, B. Su, Fabrication and characterisation of a novel biomimetic anisotropic ceramic/polymer-infiltrated composite material, Dent. Mater. 34 (2018) 994–1002.

[32] R. Chen, M. B. Johnson, K. P. Plucknett, M.-A. White, Thermal conductivity of tunable lamellar aluminum oxide/polymethyl methacrylate hybrid composites, J. Mater. Res. 27 (2012) 1869–1876.

[33] M. Petrini, M. Ferrante, B. Su, Fabrication and characterization of biomimetic ceramic/polymer composite materials for dental restoration., Dent. Mater. 29 (2013) 375–81.

[34] S. Flauder, R. Sajzew, F. A. Müller, Mechanical Properties of Porous β-Tricalcium Phosphate Composites Prepared by Ice-Templating and Poly(ϵ-caprolactone) Impregnation., ACS Appl. Mater. Interfaces 7 (2015) 845–51.

[35] S. Deville, E. Maire, A. Lasalle, A. Bogner, C. Gauthier, J. Leloup, C. Guizard, In Situ X-Ray Radiography and Tomography Observations of the Solidification of Aqueous Alumina Particle Suspensions-Part I: Initial Instants, J. Am. Ceram. Soc. 92 (2009) 2489–2496.

[36] A. Lichtner, D. Roussel, D. Jauffrès, C. L. Martin, R. K. Bordia, Effect of Macropore Anisotropy on the Mechanical Response of Hierarchically Porous Ceramics, J. Am. Ceram. Soc. 99 (2016) 979–987.

[37] S. Deville, Ice-Templated Materials: Polymers, Ceramics, Metals and Their Composites, in: Freez. Colloids Obs. Princ. Control. Use, Springer International Publishing, 2017, pp. 253–350.

[38] J.-Y. Buffiere, E. Maire, J. Adrien, J.-P. Masse, E. Boller, In situ experiments

with x ray tomography: an attractive tool for experimental mechanics, Experimental mechanics 50 (2010) 289–305.

[39] M. Peroglio, L. Gremillard, C. Gauthier, L. Chazeau, S. Verrier, M. Alini, J. Chevalier, Mechanical properties and cytocompatibility of poly(e-caprolactone)- infiltrated biphasic calcium phosphate scaffolds with bimodal pore distribution, Acta Biomaterialia 6 (2010) 4369–4379.

[40] T. P. Niebel, F. Bouville, D. Kokkinis, A. R. Studart, Role of the polymer phase in the mechanics of nacre-like composites, Journal of the Mechanics and Physics of Solids (2016).

[41] F. J. Martinez-Vazquez, F. H. Perera, I. Van Der Meulen, A. Heise, A. Pajares, P. Miranda, Impregnation of β-tricalcium phosphate robocast scaffolds by in situ polymerization, Journal of Biomedical Materials Research - Part A 101 (2013) 3086–3096.

[42] R. K. Nalla, J. H. Kinney, R. O. Ritchie, Mechanistic fracture criteria for the failure of human cortical bone., Nature materials 2 (2003) 164–8.

[43] R. K. Nalla, J. S. Stölken, J. H. Kinney, R. O. Ritchie, Fracture in human cortical bone: Local fracture criteria and toughening mechanisms, Journal of Biomechanics 38 (2005) 1517–1525.

[44] J. D. Currey, Role of collagen and other organics in the mechanical properties of bone, Osteoporosis International 14 (2003) 29–36.

[45] M. M. Porter, P. Niksiar, J. McKittrick, Microstructural Control of Colloidal-Based Ceramics by Directional Solidification Under Weak Magnetic Fields, J. Am. Ceram. Soc. 99 (2016) 1917–1926.

[46] J. Schindelin, I. Arganda-Carreras, E. Frise, V. Kaynig, M. Longair, T. Pietzsch, S. Preibisch, C. Rueden, S. Saalfeld, B. Schmid, et al., Fiji: an open-

source platform for biological-image analysis, Nature methods 9 (2012) 676–682.

[47] T. P. Niebel, F. Bouville, D. Kokkinis, A. R. Studart, Role of the polymer phase in the mechanics of nacre-like composites, J. Mech. Phys. Solids 96 (2016) 133–146.